YNCenter Video Conference

Quantifying gas ebullition with echosounder: the role of methane transport by bubbles in a medium-sized lake

I. Ostrovsky*et al.*, 2008

Reporter: Wang Jiao
2017.09.22

Outline

- Background
- Materials and procedures
- Results and Discussion
- Conclusion

Background

The emission of highly potent greenhouse gases has contributed to the increased atmospheric concentration of methane by approximately 1% per year over the last century (Rowland 1985).

Point-source ebullition from shallow lakes is a dominant (and previously unrecognized) source of methane emission to the atmosphere.

As lakes (especially in the northern hemisphere) are a prominent landscape feature, methane ebullition is a much larger and globally significant source of atmospheric methane than formerly thought (St. Louis et al. 2000; Bastviken et al. 2004; Walter et al. 2007).

Materials and procedures

	Location	Dual-beam echosounder	Pulse width	Ping rate	Lower threshold for data collection	Data collection
Laboratory experiments	a large outdoor tank	120 KHz	0.2 ms	10pings s^{-1}	-80 dB	between 0.5 m above the bottom to 1 m from the transducer
field study	in Lake Kinneret	120 KHz	0.1 or 0.2 ms	5pings s^{-1}	-75 dB	between 1 m from the transducer to 0.5 m above the bottom

Laboratory setup

- Fresh Lake Kinneret water
- Water temperatures between 17℃ and 21℃
- Bubble Measurement/Control System(BMCS)
- Biosonics dual-beam scientific echosounder DE5000
- Acoustic transducer/receiver

Laboratory setup

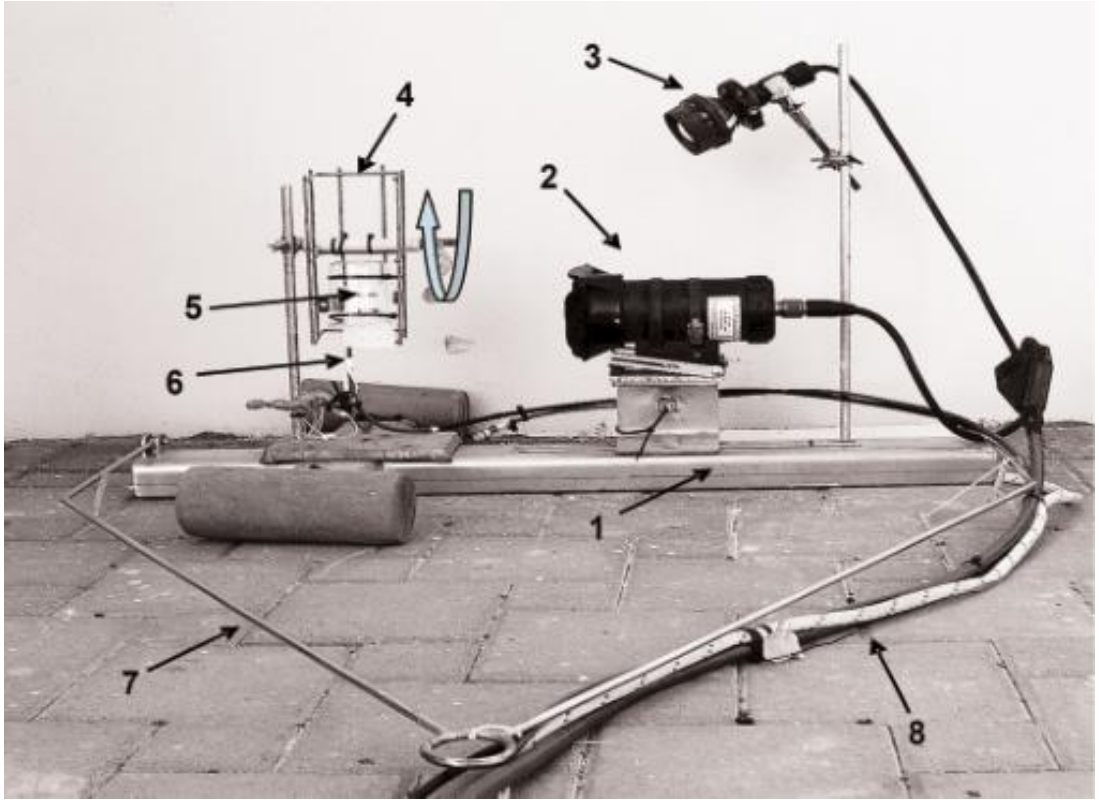

structural
imaging
illumination
data acquisition

Fig. 1. Experimental setup: BMCS. 1, stainless steel platform; 2, video camera mounted on a movable chariot; 3, source of light; 4, rotating frame; 5, volumetric beaker; 6, outlet of the air tube; 7, stain-less steel frame; 8, cables (rope + electronic cable + high-pressure air tube).

Results and Discussion

In the following section, it is necessary to first determine the empiric relationships between gas volumes, acoustic sizes, and rise velocities of individual bubbles in laboratory conditions. This information is then applied to the lake to determine gaseous methane flux from the bottom.

A : Acoustic size of bubbles

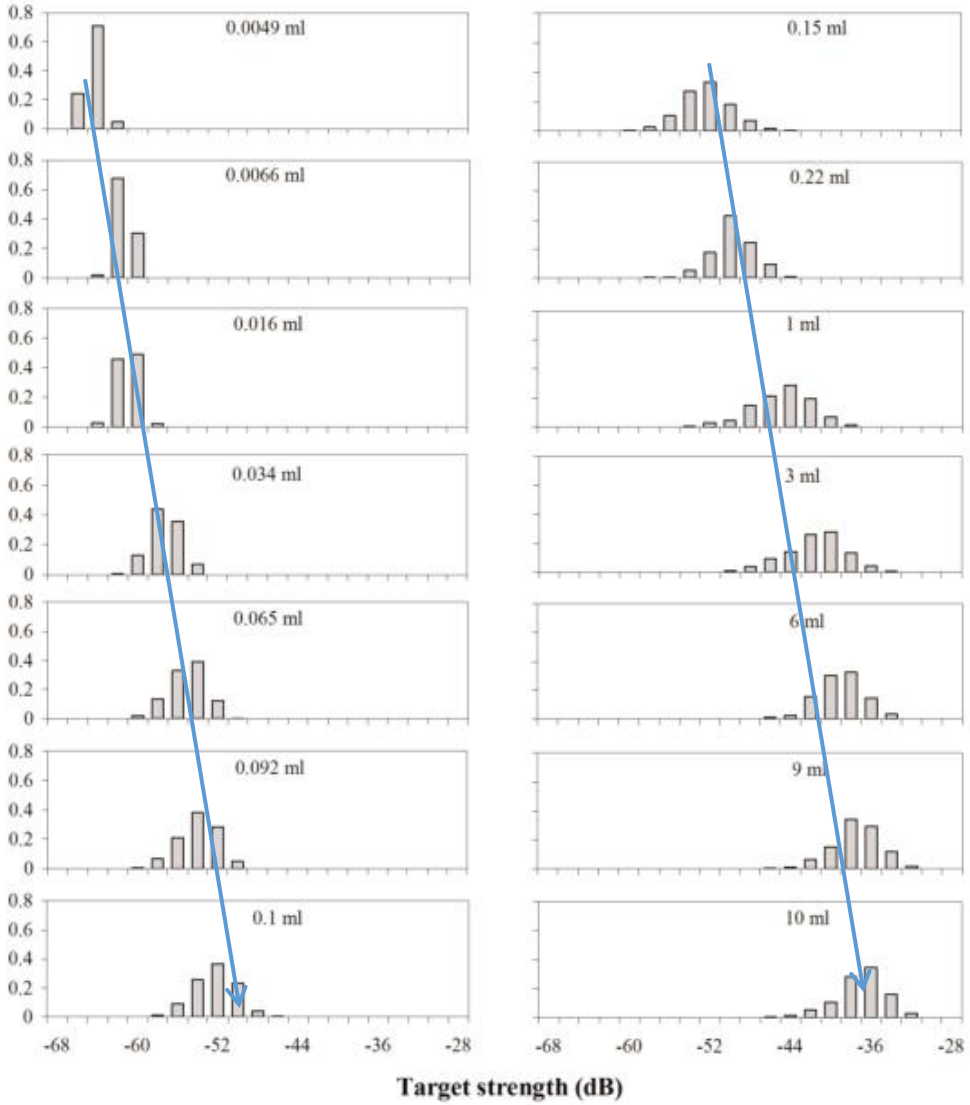

Fig. 2. Target strength distribution for bubbles of different volumes. Each histogram was based on more than 240 measurements.

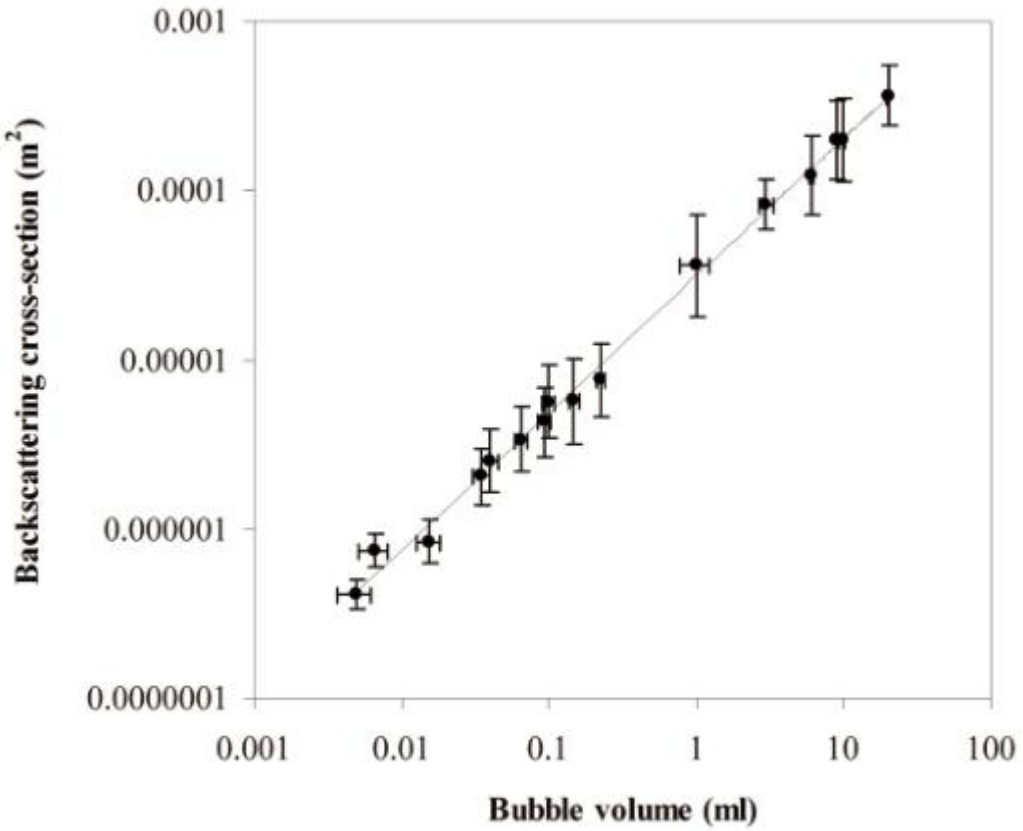

Fig. 3. Relationships between backscattering crosssection, σ_{bs}, and volume of bubbles. Each point represents the average σ_{bs} for measured bubble volumes. Line represents best fit using liner regression of log transformed values (Eq. 1a). Bars represent means $\pm$ SD.

For bubbles ranging from 0.005 to 20 mL, the empiric relationship between σ_{bs} and volume can be accurately described by a logarithmic equation :

- $\log(\sigma_{bs}) = (0.745 \pm 0.013)\log(V) - (4.467 \pm 0.016)$ (1)

  or

- $\sigma_{bs} = 3.409\ 10^{-5}\ V^{0.745 \pm 0.013}$ (1a)

- $TS = 10\log(\sigma_{bs}) = 7.45\log(V) - 44.67$ (2)

- $V = 995600\ \sigma_{bs}^{1.3426}$ (3)

  and

- $V = 995600\ e^{0.3092\ TS}$ (4)

TS is target strength

B : Bubble allometry

The ratio of the horizontal radius to the vertical radius is an aspect ratio ($AR = r_h / r_v$), which indicates how much a particular bubble is vertically flattened.

$$AR = r_h / r_v$$

(r_{eq} is equivalent radius: $r_{eq}^3 = r_h^2 r_v$)

$$AR = r_h r_v^{-1} = r_h (r_{eq}^{-3} r_h^2) = r_h^3 r_{eq}^{-3} \quad (5)$$

($r_h^3 \sim \sigma_{bs}^{3/2}$ and $r_{eq}^3 \sim V$)

$$AR = r_h^3 r_{eq}^{-3} \sim \sigma_{bs}^{3/2} V^{-1} = AR' \quad (6)$$

$$AR' = \sigma_{bs}^{3/2} V^{-1} = 0.199\, V^{0.117} \quad (7)$$

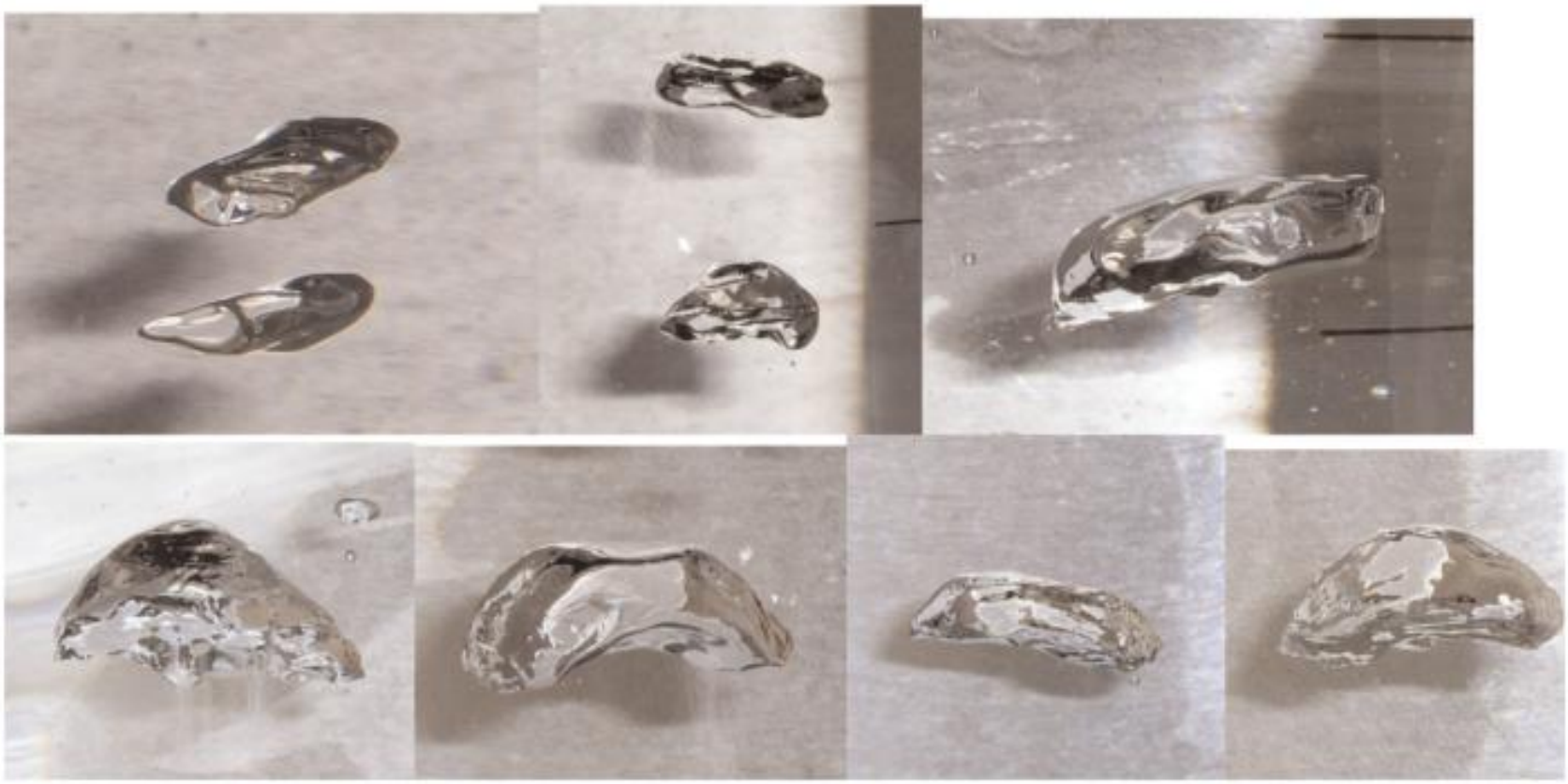

Fig. 4. Photo of rising bubbles of 1 to 3 mL demonstrating the variability in shape.

C : Rise velocity

$$v = -(0.00219 \pm 0.00093)(\log V)^4 - (0.000737 \pm 0.00091)(\log V)^3 + (0.04413 \pm 0.0050)(\log V)^2 + (0.0662 \pm 0.0034)\log V + (0.2663 \pm 0.0050) \quad (8)$$

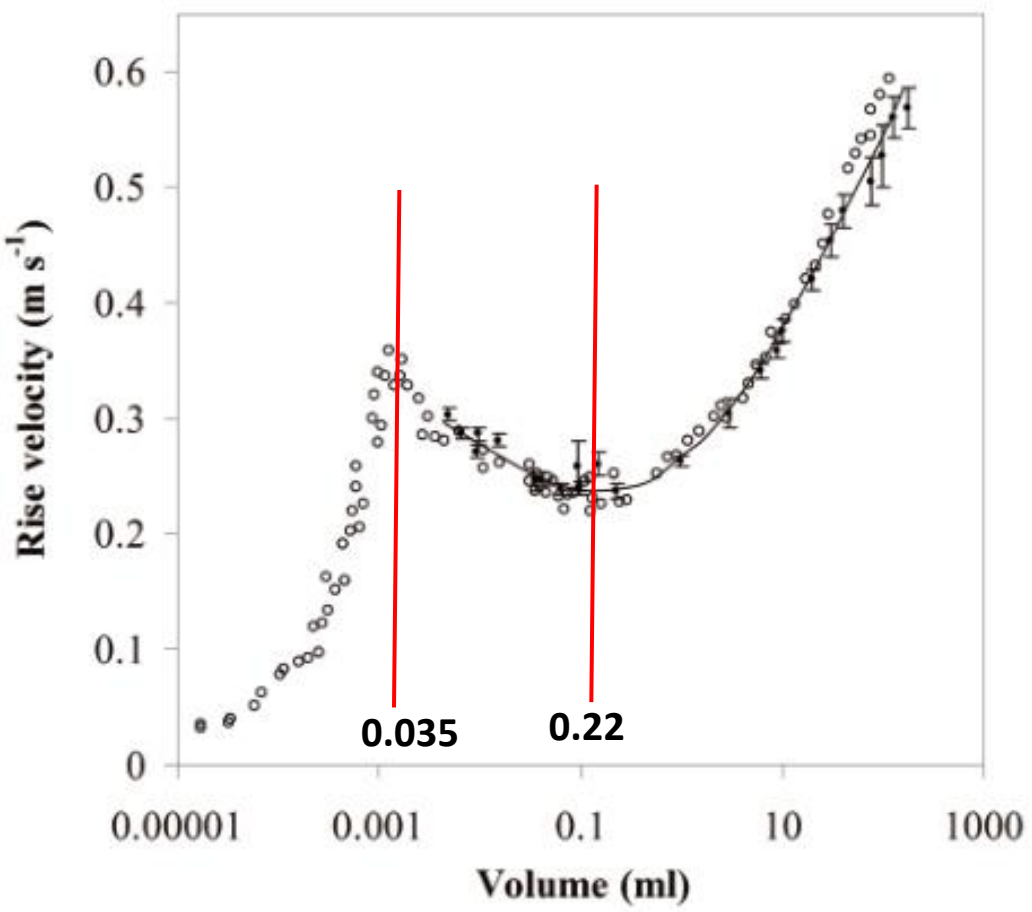

Fig. 5. Relationships between rise velocity and bubble volume. Empty circles are data obtained for tap water at 20℃ by Haberman and Morton (1954).

Reconstruction of bubble size distribution in a lake

The reconstruction of bubble volume distribution was performed using a deconvolution algorithm for positive signals (e.g., Hovorka et al. 1998; Morhac and Matousek 2005) based on the TS-frequency distribution measured in nature and two transfer functions:

(a) the TS-V relationship

(b) dispersion of the measured TS for bubbles of different sizes

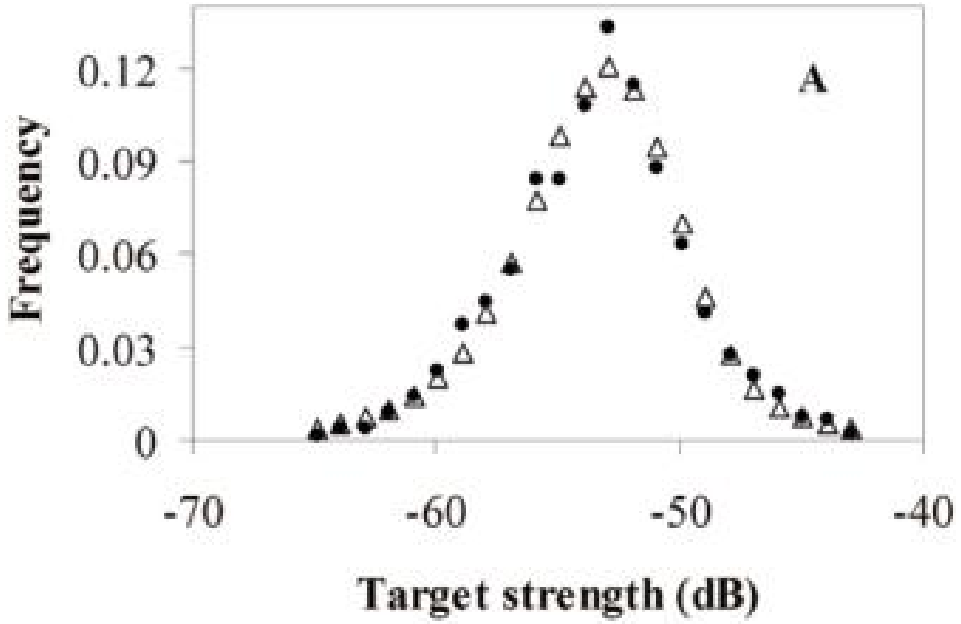

- **hydroacoustic data**
- △ **back-calculated TS distribution**

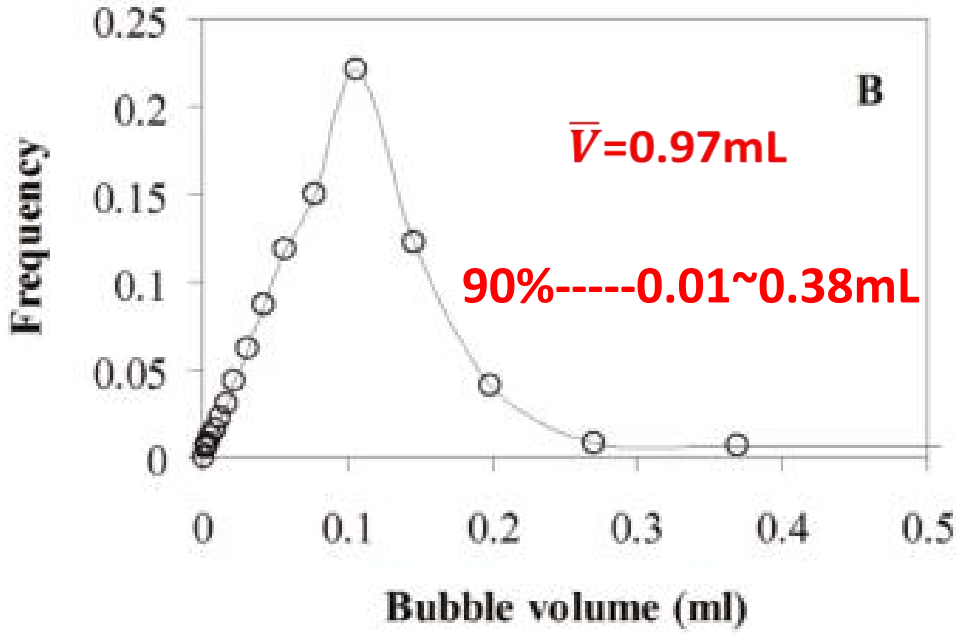

Fig. 6. Size distributions of bubbles in the hypolimnion of Lake Kinneret on 16 October 2001. (A) TS-frequency distributions. (B) Volume-frequency distribution obtained using a deconvolution procedure.

D : Quantification of bubble abundance

The volumetric concentration of bubbles in water, $V_{\Sigma B}$, (mL m^{-3}), is a product of bubble density, N (ind. bubbles m^{-3}) and the average volume of bubbles, V (ml). Then, the $V_{\Sigma B}$ can be quantified as

$$V_{\Sigma B} = NV = (S_U \sigma_{bs}^{-1}) (995600 \sigma_{bs}^{1.3426}) = 542100 S_U \sigma_{bs}^{0.3426} \quad (9)$$

$$V_{\Sigma B} \approx 13500 S_U \quad (10)$$

E: Gaseous methane flux

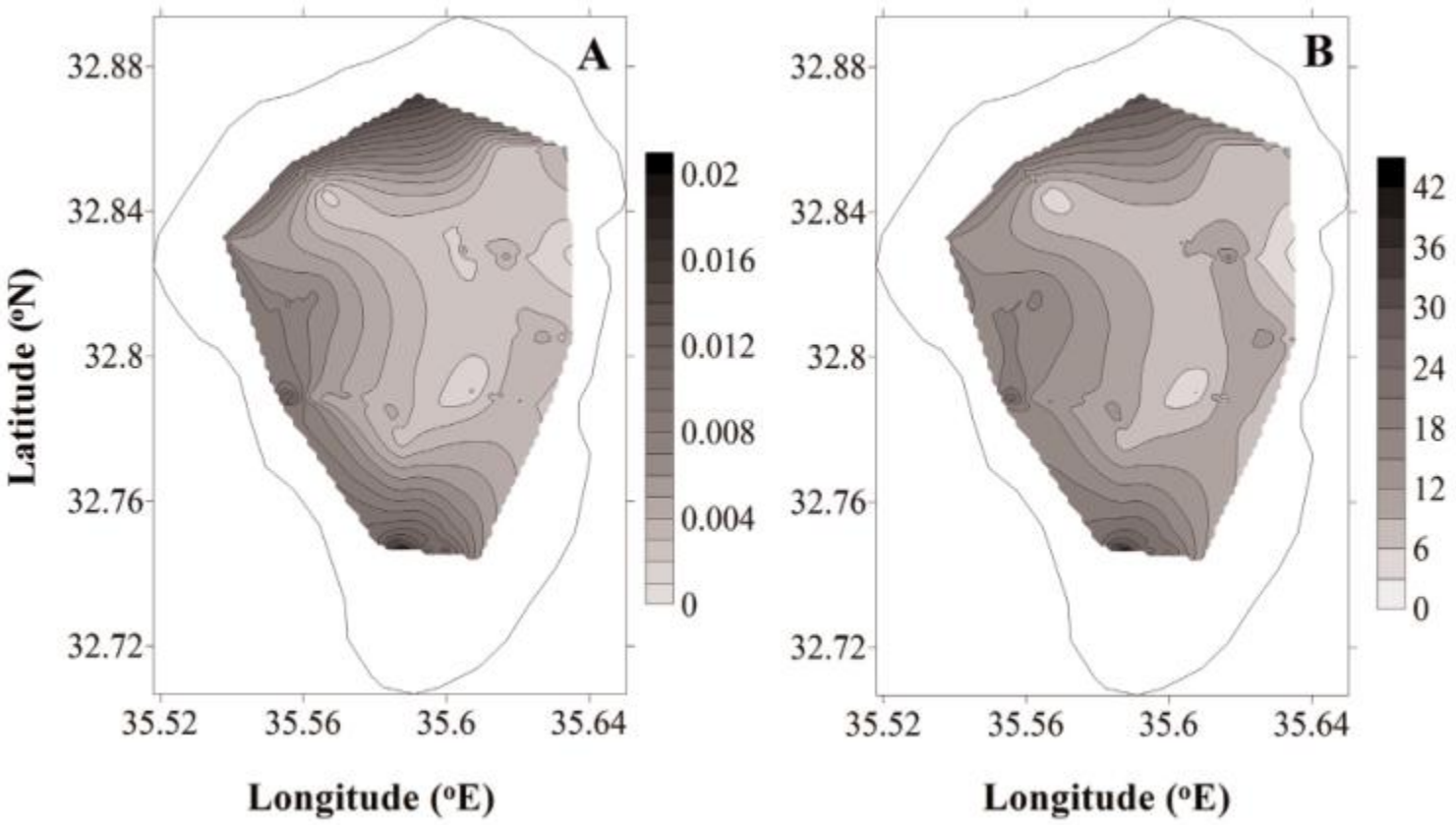

Fig. 7. Spatial variability in the volumetric concentration of bubbles (mL m^{-3}) in the near-bottom water layer (A) and gaseous methane flux (mmol m^{-2} d^{-1}) from the bottom (B) in Lake Kinneret on 2 August 2001.

Conclusion

The fate of methane released from the sediment in bubbles strongly depends on the initial bubble size.

σ_{bs} is proportional to $V^{0.745}$, which also suggests an allometric change in bubble shape with size: larger bubbles became more flattened.

The bubble rise velocity, which is necessary for the calculation of the gaseous methane flux from sediments, strongly depends on bubble size and purity of the bubble surface.

In fact, the data showed that the backscattering strengths of bubble population correlate well with the total volume of bubbles in the water column, at least in the cases where sizes of bubbles do not vary much.

Method applicability

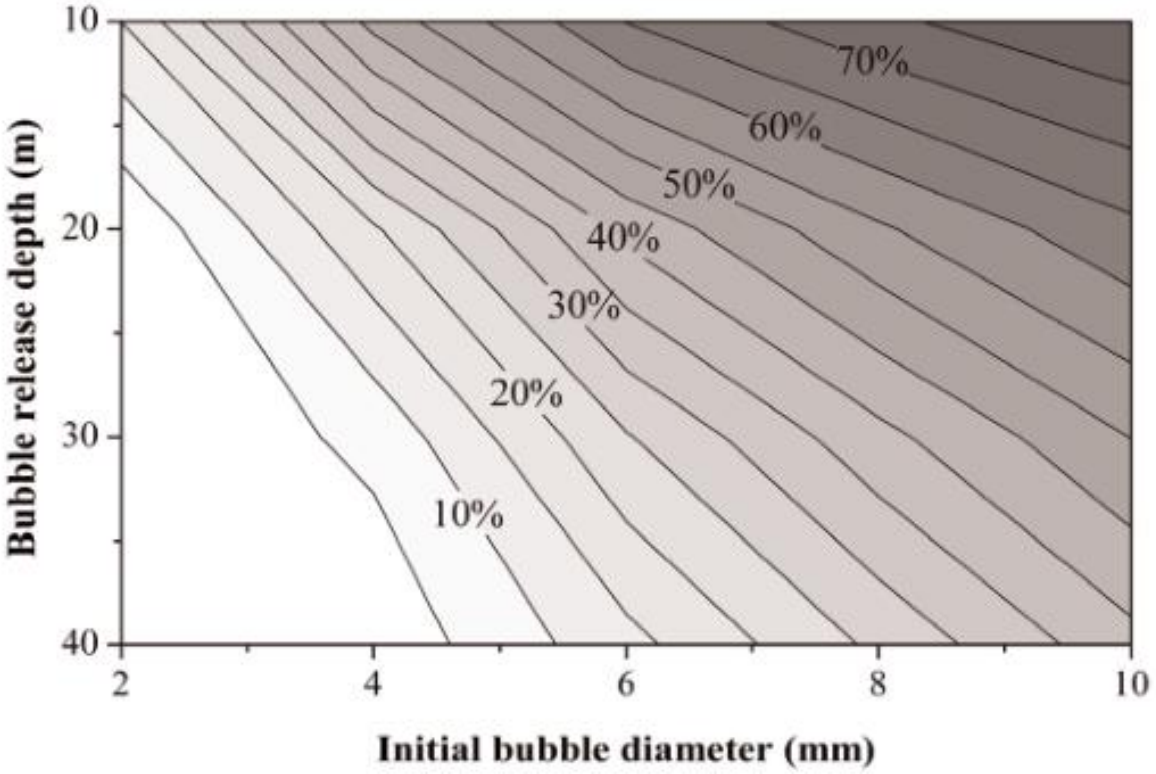

For a pure methane bubble, Fig. 8 shows the relationship between bubble release depths, initial bubble size, and amount ultimately reaching the atmosphere.

Fig. 8. Contour plot developed from bubble model of McGinnis et al. (2006)

Method applicability

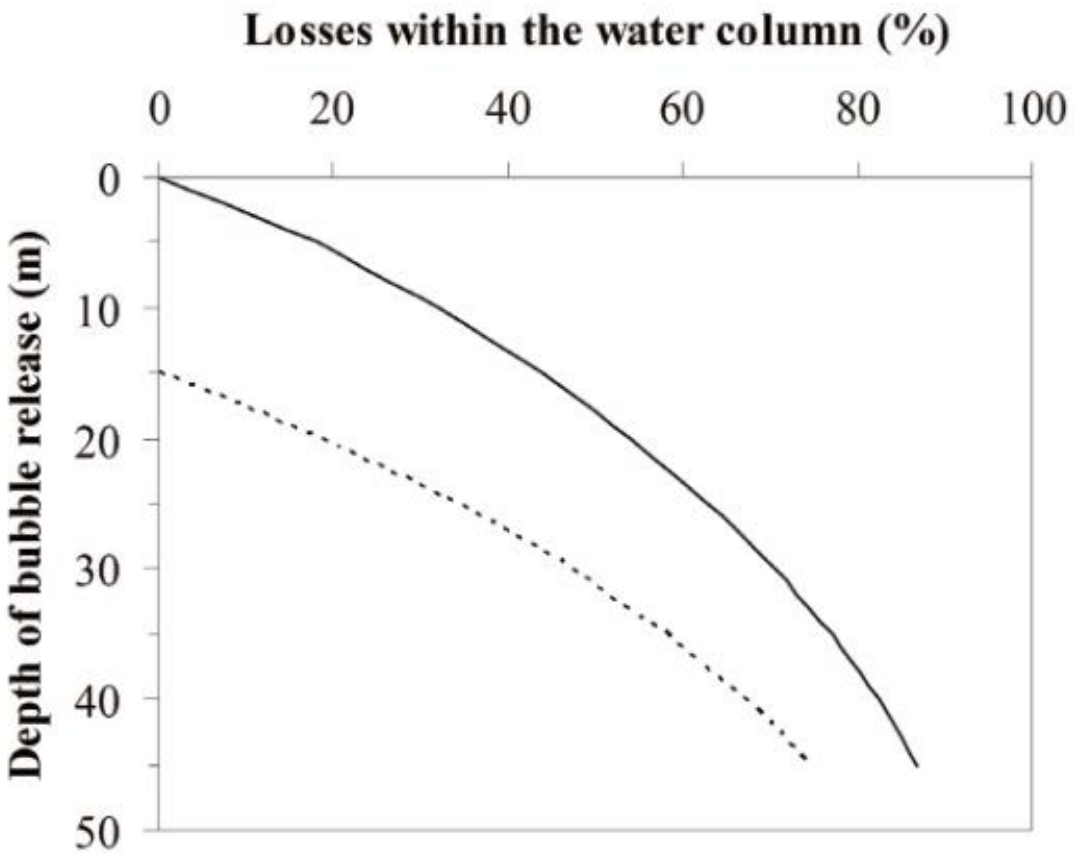

losses within the entire water column

losses within the hypolimnion

Fig. 9. Losses of methane from bubbles released from different depths.Calculations were done based on gas exchange model (McGinnis et al. 2006) applied to 3 mm (in radius) bubbles.

Thanks for your attention!